The Effect of the Preferential Affinity of the Solvent on the Microstructure of Solution-Cast Block Copolymer Thin Films

Yuhu Li, Haiying Huang, and Tianbai He*

State Key Laboratory of Polymer Physics and Chemistry, Changchun Institute of Applied Chemistry, Chinese Academy of Sciences, Changchun, 130022, P. R. China

Yumei Gong*

School of Chemical and Material, Dalian Polytechnic University, Dalian, 116034, P. R. China

Received: September 13, 2009; Revised Manuscript Received: November 25, 2009

We have studied the microstructures of the solvent-cast films of polystyrene-*block*-poly(methyl methacrylate) (PS-*b*-PMMA) diblock copolymer with PMMA cylinder-forming composition. The casting solvents, 1,1,2-trichloroethane (TCE), toluene (Tol) and their binary mixtures, were controlled to evaporate at a certain rate $R \approx 0.01$ mL/h, and the effect of the preferential affinity of the solvents for a certain block P2VPng microstructures is investigated. 1,1,2-Trichloroethane and toluene, with similar volatility, are good solvents for both PS and PMMA blocks but having opposite preferential affinity for each block (TCE has preferential affinity for the minority PMMA block and Tol has preferential affinity for the majority PS block), and the preferential affinity of the solvents is modulated by mixing the two solvents. As the preferential affinity of the solvents for the majority PS block increases, a series of microstructures including perforated lamella with ringlike morphologies, PMMA cylinders, PMMA spheres, and PMMA cylinders covered with a layer of PS microdomain have been observed. The results are discussed in view of the effective volume fraction of each block induced by the solvent preferential affinity and the special mechanical strain field brought by the solvent evaporation.

Introduction

Block copolymers can self-assemble into diverse well-ordered microstructures on the nanometer scale ranging from spheres, cylinders, perforated lamella, gyroid, and lamella depending on the volume fractions of blocks.[1−3] The fascinating characteristic has captured much attention of scientists and technologists over the past decades from both the experimental and the theoretical owing to the application in date storage, electronics, combinatorial chemistry, masks, and membranes, etc.[3−6] A lot of methods have been used to control and manipulate the microstructures of the block copolymer thin films, such as modulating the nature of solvent,[7,8] controlling the solvent evaporation rate,[9−16] solvent annealing,[17−20] using electric fields,[21,22] varying the films thickness,[10,23−26] etc.

Solvent evaporation is an effective and direct approach to modulate the microstructures of block copolymer thin films in which both the nature of solvent and the evaporation rate (R) are crucial factors. The nature of solvent influences the degree of the swelling of each block and accordingly has severe effects on the resulting block copolymer microstructures. Inoue et al.[7] showed that the microstructures of polystyrene−polyisoprene diblock copolymer films varied from spherical to lamellar phase depending on the nature of the solvent used in the casting process. Funaki et al.[8] also investigated the effect of different solvents on the resulting microstructures in the thin films of a poly(2-vinylpyridine)-polyisoprene (P2VP-*b*-PI) diblock copolymer and found that cylindrical phase ($f_{P2VP} = 0.12$, where f_{P2VP} represents the volume fraction of block P2VP in the block copolymer) and spherical and lamellar phases ($f_{P2VP} = 0.26$) were obtained depending on the nature of the casting solvents. On the other hand, once the solvent is selected, the evaporation rate is the key factor to control the resultant microstructures. Kim and Libera[9] showed that PS cylinders can be oriented either perpendicular or parallel in the film of polystyrene−polybutadiene−polystyrene triblock copolymer with 30 wt % PS depending on the solvent evaporation rate. Fukunaga and Elbs[11] investigated the effect of the solvent removal speed on the resulting microstructures in the films of a polystyrene-poly(2-vinylpyridine)-poly(*tert*-butyl methacrylate) triblock copolymer and the perpendicular and parallel orientations of lamella were obtained at fast and slow solvent removal speed, respectively. Our group's previous work[12−16] on cylinder forming block copolymers demonstrated that unconventional inverted phase (the majority block in a matrix of the minority block), equilibrium normal phase (the minority block in a matrix of the majority block), and ring-shaped phase could be obtained by controlling the solvent evaporation rate.

Although solvent evaporation has been widely used, the details remain rather unclear since the relevant experimental parameters governing the drying process (nature of solvent, partial pressure of solvent, amount of solvent uptake, rate of solvent evaporation, etc.) are usually complex and difficult to control. In the present work, we explore the thin film microstructures of a cylinder-forming polystyrene-*b*-poly(methyl methacrylate) (PS-*b*-PMMA) diblock copolymer cast from 1,1,2-trichloroethane (TCE), toluene (Tol), and their binary mixture solutions by controlling the solvent to evaporate at a certain rate $R \approx 0.01$ mL/h. The advantage of the solvents is that both

* To whom correspondence should be addressed. (T.H.) E-mail: tbhe@ciac.jl.cn. Fax: +86 431 85262126. Tel.: +86 431 85262123. (Y.G.) E-mail: ymgong@dlpu.edu.cn. Fax: +86 411 86323736. Tel: +86 411 82392818.

10.1021/jp908852u
Published on Web 12/31/2009

TABLE 1: Characteristics of the Casting Solvents

	solubility parameter[a]	molar volume[b]	boiling temperature[b]	vapor pressure[b]
	δ (J/cm^3)$^{1/2}$	V (cm^3/mol)	T_b (°C)	(kPa)
TCE	20.3	92.5	114	4.80 (30 °C)
Tol	18.3	106.3	111	4.00 (26 °C)

[a] Obtained from Polymer Handbook, 4th ed.[43] [b] Obtained from Solvents Handbook, 4th ed.[48]

(TCE and Tol) have opposite preferential affinity for each block (TCE has preferential affinity for the minority PMMA block and Tol has preferential affinity for the majority PS block) and similar vapor pressure (~4 kPa) at room temperature, which allow us to obtain binary mixtures of the two solvents with different preferential affinity for each block in detail and keep the nature of the solvent binary mixture invariable during the solvent evaporation process easily. We shall show that quite different thin film microstructures can form depending on the preferential affinity of the casting solvent after complete solvent evaporation. What is the most intriguing is that the microstructure observed at the solvent preferential affinity for the minority PMMA block is perforated lamellar phase with ring-shaped morphology. Existence of perforated lamellar phase in block copolymer bulk and film has been theoretically predicted and experimentally observed by several research groups.[10,23,24,27−41] In this paper, however, we report the perforated lamellar phase with ring-shaped morphology trapped in solvent casting thin films of a diblock copolymer consisting of the layer of the cylinder forming PMMA block perforated by ring-shaped channels of the majority PS block. The effective volume fraction of each block associated with the solvent preferential affinity and the kinetics of solvent evaporation are expected to be responsible for the interesting microstructure formation. A direct observation of the perforated lamellar phase with ring-shaped morphology dominating microstructure shown in this work will offer a good example to refine the input parameters to the theory and simulation and to test the predictions against the results under other conditions in block copolymer research.

Experimental Section

Materials. An asymmetric diblock copolymer used in this work PS_{1411}-*b*-$PMMA_{540}$ (the numbers in subscript refer to the number-average degree of polymerization of each block) with polydispersity index 1.10 was purchased from Polymer Source Inc. and used as received. In bulk state, this block copolymer adopts hexagonally packed PMMA cylinders with a center-to-center distance (the period L_0) about 65 nm embedded in a PS matrix, confirmed by small-angle X-ray scattering (SAXS). Two solvents, 1,1,2-trichloroethane (TCE) and toluene (Tol), were used to dissolve the block copolymer. The characteristics of the two solvents are listed in Table 1. Moreover, binary mixtures of the two solvents are also used to dissolve the block copolymer. Each solvent mixture was prepared volumetrically at room temperature, ignoring possible volume changes upon mixing.

Sample Preparation. ***Solution-Cast Films.*** The diblock copolymer was dissolved in TCE, Tol, and their binary mixtures separately to yield 1 mg/mL solutions. In the experiment, a 15 μL pipet was used to cast equal-sized droplets of the solution onto carbon-coated mica (1.5 × 1.5 cm^2). Then the films were dried at a certain solvent evaporation rate ($R \approx 0.01$ mL/h) under room temperature (~25 °C) until no further weight loss was detected. It takes ~1.5 h to obtain a dry film. The evaporation rate ($R \approx 0.01$ mL/h) was achieved by placing solution-cast films on a big and flat glass, and then covered with a glass dish with 5 cm in radius and 3 cm in height. During the whole evaporation process, although the solvent evaporation rate slows down as the solvent in the casting film decreases, we can deem that the composition of the solvent binary mixture is invariable because TCE and Tol have similar vapor pressure (~4 kPa) at room temperature. That is, the nature of the solvent binary mixture is invariable during the evaporation process. After completely dried, the thickness of the as-cast film was about 70−80 nm. This film thickness is within the film boundary effects extending distance about one microdomain spacing 65 nm for the present block copolymer.[12] However, the carbon coating locates on the substrate[25] and the fact that the temporal film thickness during the film drying process is much larger than that of the dried film can decrease some of the boundary effect of the substrate. Therefore, the performed experiment can reveal the effect of the nature of the solvent which locates in the film bulk and covers the film surface during the evaporation process on the microstructures of the solvent-cast block copolymer film.

Spin-Casting Films. The diblock copolymer was dissolved in Tol to yield 10 mg/mL solution and then the solution was spin-coated onto carbon-coated mica at 2000 rpm for 30 s to get a film with ~70 nm in thickness. After removal of the residual solvent under vacuum at room temperature for 24 h, the film was annealed under vacuum at 180 °C for 48 h and quenched to room temperature for TEM examination.

Instruments. The microstructures of the films were examined by transmission electronic microscopy (TEM) and X-ray photoelectron spectroscopy (XPS). TEM experiments were performed on a JEOL 1011 TEM with an accelerating voltage of 100 kV in the bright-field mode. For plain-view TEM observation, the thin film and its carbon support were floated off onto a pool of distilled water and then picked up with copper grids. To enhance the contrast between the PS and PMMA phases, the specimens were stained with RuO_4 for several hours prior to observation. Since RuO_4 selectively reacted with the phenyl of the PS blocks, the PS microdomains appear dark and the PMMA microdomains appear bright in the TEM micrographs. For cross-sectional TEM experiments, some portions of the floated film were collected onto a piece of cured epoxy resin and dried. After staining with RuO_4, these epoxy pieces were coated with a thin layer of carbon, and then these epoxy pieces (epoxy + carbon layer + polymer film + carbon layer) were embedded in epoxy resin and subsequently heated to 35, 45, and 55 °C, respectively for 12 h. The ultrathin sections with approximately 60 nm in thickness were microtomed using a LEICA Ultracut R microtome and a glass knife at room temperature and collected onto the carbon-coated copper grids. Finally, the specimens of ultrathin sections were stained with RuO_4 for several hours again prior to observation.

X-ray Photoelectron Spectroscopy (XPS). The surface chemical composition of thin films was determined by a VG ESCALAB MKII spectrometer with a Mg X-ray source. Pass energy of 20 eV was used to obtain the high resolution, and the takeoff angle of the X-ray source was 90°. The main chamber of the XPS instrument was maintained at 2.0×10^{-7} Pa during the spectral measurements.

Results and Discussion

For a given system, the relative affinity of a solvent for each block can be estimated from the polymer−solvent interaction parameter $\chi_{P-S} = V_S(\delta_S - \delta_P)^2/RT + 0.34$,[42,43] where P

TABLE 2: Polymer−Solvent Interaction Parameters (χ) Calculated from Different Pairs of Polymers and Solvents

	PS	PMMA
TCE	0.448	0.385
Tol	0.344	0.374

TABLE 3: Preferential Affinity of the Binary Mixtures of the Solvents

V_{tce}/V_{tol}	100/0	90/10	70/30	50/50	30/70	10/90	0/100
$\Delta\chi$	−0.063	−0.054	−0.037	−0.020	0	0.021	0.030

TABLE 4: Microstructures of the Block Copolymer as a Function of the Preferential Affinity of the Solvents[a]

$\Delta\chi$	−0.063 to −0.037	−0.020	0	0.021	0.030
microstructure	PLR	TS	C and S	S	CC

[a] PLR = perforated lamella with ring-like morphologies; TS = transitional structure from perforated lamella to cylinder; C and S = hybrid structure of PMMA cylinders and PMMA spheres; S = PMMA spheres; CC= PMMA cylinders covered with a layer of PS microdomain.

represents polymer, *S* represents solvent, *Vs* is the molar volume of solvent, *R* is the gas constant, *T* is the temperature, and δs and δ_P are the solubility parameters of the solvent and polymer, respectively. In the present system, the solubility parameters of the solvents are listed in Table 1, and those of polymers are $\delta_{PS} = 18.6$ (J/cm^3)$^{1/2}$, and $\delta_{PMMA} = 19.2$ (J/cm^3)$^{1/2}$, respectively. The calculated polymer−solvent interaction parameters (χ) for different pairs of polymers and solvents at room temperature are shown in Table 2. According to the Flory−Huggins theory criterion, polymer and solvent are completely miscible over the entire composition range when the obtained value $\chi < 0.5$. Hence, the two solvents with similar volatility used in this work should be good solvents for both PS and PMMA blocks but having opposite preferential affinity for each block, TCE has preferential affinity for the minority PMMA block and Tol has preferential affinity for the majority PS block. Therefore, the binary mixtures of the two solvents are good for both blocks, and the preferential affinity of the binary mixtures can be modulated by changing the mixing volume fraction of the two solvents. Moreover, since both solvents have similar volatility, the composition and the nature of the binary mixtures of the two solvents can be considered invariable with the evaporation. The solubility parameter and the molar volume of the binary mixture of the two solvents are taken as the sum of the products of the component value with their volume fractions:[43] $\delta_{mixture} = \Sigma\delta_i\Phi_i$ and $V_{mixture} = \Sigma V_j\Phi_j$, where Φ_i and Φ_j are the volume fractions of the solvents in the mixture. An expression $\Delta\chi = \chi_{S\text{-}PMMA} - \chi_{S\text{-}PS}$ is used in representing the preferential affinity of a solvent for a certain block. That is, $\Delta\chi < 0$, $\Delta\chi = 0$, and $\Delta\chi > 0$ indicate the solvent has preferential affinity for the minority PMMA block, is neutral for each block, and has preferential affinity for the majority PS block, respectively. The characteristics of all the solvents used in this work are listed in Table 3. According to the value of $\Delta\chi$, with a decrease in the volume ratio of TCE/Tol (V_{TCE}/V_{Tol}) from 100/0, 90/10, 70/30, 50/50, 30/70, 10/90, to 0/100, the preferential affinity of the binary mixtures of the two solvents for the majority PS block increases.

In Table 4, we summarize the microstructures of the thin films cast from the above binary solvent mixtures dried at solvent evaporation rate $R \approx 0.01$ mL/h. As is shown, with the preferential affinity of the casting solvents for the majority PS block increasing, complex microstructures including perforated lamella with ring-like morphologies, PMMA cylinders, PMMA spheres, and PMMA cylinders covered with a layer of PS microdomain were obtained. The results can be divided into three parts according to the preferential affinity features of the solvents: $\Delta\chi < 0$ in the first part, $\Delta\chi = 0$ in the ensuing part, and $\Delta\chi > 0$ in the third part.

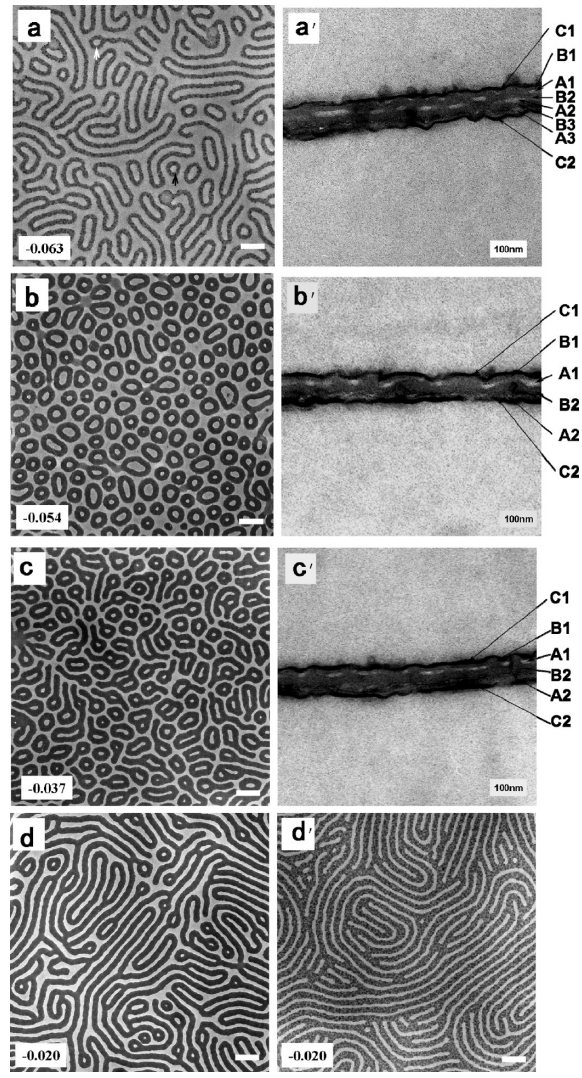

Figure 1. TEM micrographs of the films cast from the solvents with preferential affinity for the minority PMMA block ($\Delta\chi < 0$) at the solvent evaporation rate $R \approx 0.01$ mL/h. The preferential affinities of the solvents are (a and a′) −0.063, (b and b′) −0.054, (c and c′) −0.037, and (d and d′) −0.020, respectively. The panels a′, b′, and c′ show the cross-sectional TEM micrographs corresponding to plane-view micrographs in panels a, b, and c, respectively. The black and white arrows in panel a exhibit normal ring and tail-attached ring, respectively. Scale bar for the plane-view micrographs: 200 nm.

$\Delta\chi < 0$: The Solvents Have Preferential Affinity for the Minority PMMA Block. Figure 1 shows the TEM micrographs of the block copolymer films cast from the solvents with preferential affinity for the minority PMMA block ($\Delta\chi < 0$) dried at the solvent evaporation rate $R \approx 0.01$ mL/h. Obviously, as the value of $\Delta\chi$ increases from −0.063 (corresponding to the TEM micrographs as shown in Figures 1a and 1a′) to −0.020 (corresponding to the TEM micrographs as shown in Figure 1 panels d and d′), that is, as the preferential affinity of the casting solvents for the minority PMMA block decreases, a series of complex microstructures are observed. The plane-view TEM micrograph in Figure 1a gives the microstructure of the film cast from the solvent with $\Delta\chi = -0.063$ (pure TCE) dried at

the solvent evaporation rate $R \approx 0.01$ mL/h. It shows that the dominating morphology is elongated ring-shaped, including a few normal rings and tail-attached rings, shown in the Figure 1a by black and white arrows, respectively. A feature shared by all the rings is a uniform dark ring rod width of 50 ± 2 nm and a uniform ring inner region width of 65 ± 2 nm, determined from the TEM micrograph in Figure 1a. Since the dark regions are RuO_4 selectively stained PS and the bright are PMMA in the TEM micrograph of PS and PMMA, we can deduce that the majority PS block forms elongated rings dispersing in a PMMA matrix in Figure 1a. But the cross-sectional TEM micrograph of this film in Figure 1a′ shows that the bright PMMA forms the dispersed microdomain in which the two black layers marked by C1 and C2 sandwiching the film are the carbon coatings introduced during the sample preparation and the dark regions marked by B (B1, B2, and B3) surrounding the PMMA microdomain is PS, with 4−5 nm in thickness of B1 sandwiched by the black carbon layer C1 at the top of the film and the dispersed bright PMMA microdomain marked by A1 and 32 nm in thickness of B2 sandwiched by the two bright PMMA microdomains marked by A1 and A2. That is, the thickness of the layer of PS at the film surface is 4−5 nm, which is connected with B2. Figure 1a′ also shows that there is a thin layer of PMMA with 5−7 nm in thickness at the bottom of the film because the carbon-coated substrate prefers the PMMA block,[12] despite that this kind of preference may be very weak because of the existence of the carbon on the substrate. Combining these two micrographs in Figure 1 panels a and a′, the microstructure formed in the film cast from the solvent with $\Delta\chi = -0.063$ dried at the evaporation rate 0.01 mL/h is expected to be a perforated lamellar morphology, and the lamellae of the minority PMMA block are perforated by the channels of the majority PS block. Since the PS rings are elongated, the microstructure in Figure 1 panels a and a′ is defined as perforated lamella with elongated PS rings (PLR).

It is interesting to note that the perforating PS channels in the perforated lamella in Figure 1a,a′ are elongated ring or ring-shaped. The microstructure of perforated lamella has been found before in block copolymer thin films[10,23,24,27−35] and bulks,[36−41] and the perforating channels are hexagonally arranged. In thin films of a cylinder-forming block copolymer, the microstructure of perforated lamella has been explained by the depletion of the majority block if both the boundary surfaces of the film show strong enough preference to the majority block, the cylinders of the minority block connects to a perforated layer.[29] In bulk, the microstructure of perforated lamella is bounded in composition between the lamella and cylinder phases at the volume fraction of a certain block between 0.35−0.40 or 0.63−0.70, and the minority block forms a layer perforated by the channels of the majority block. In the solvent cast film in the present work, the perforated lamellar phase also consists of lamellae of the minority PMMA block perforated by the channels of the majority PS block, but the perforating channels form ring-shaped morphologies.

Previously, ring-shaped morphologies have been observed in solution-cast films of a cylinder-forming PS-*b*-PMMA block copolymer, as solvent (1,1,2,2-tetrachloroethane, a solvent with preferential affinity for PMMA) evaporates at $R \approx 0.02$ mL/h and 0.004 mL/h, in which the ring-shaped morphology is expected to be embedded in a matrix of homogeneous block copolymer and the film thickness is ∼300 nm.[12] In the present work, however, when the thickness of the film decreases to 70−80 nm, the ring-shaped morphology is perforated lamella with ringlike morphologies and there is a thin layer of PS 4−5 nm covered the film surface. It is expected that the nature of the solvent together with the mechanical strain field brought by the fast solvent evaporation ($R \approx 0.01$ mL/h) plays a crucial role in the fascinating microstructure formation.

As is known, the solvent with different nature will influence the degree of the swelling of the polymer chains in each block and hence result in different effective volume fractions of each block.[8] That is, the existence of solvent will change the effective composition of the block copolymer and such temporary composition is related to the amount of the solvent. Moreover, the state of block copolymer in solvent can be held in the film by the solvent fast evaporation, for instance, $R \approx 0.01$ mL/h, which has been confirmed by our previous work.[12] The solvent used here with $\Delta\chi = -0.063$ is good for both two blocks, but has preferential affinity for the minority PMMA block. It will diffuse into PMMA block easier and swell the PMMA block more than the PS block. Hence, the effective volume fraction of the PMMA block increases in block copolymer solution, and is larger than that in the bulk 27%. In such case, the curvature of the interface between PS and PMMA microdomains will be different from that in the bulk. When the effective volume fraction of the PMMA block is high enough and makes it form a perforated layer, the perforated lamellar microstructure forms. In this opinion, with the preferential affinity of the solvent for PMMA decreasing the content of the PS channels in the PMMA layer is expected to increase (see below). The content of PS channels calculated from the plane-view TEM micrograph in Figure 1a is ∼46%. On the other hand, in view of the surface tension of the two blocks, the layer of the minority PMMA block with higher surface tension (41.1 dyn/cm) perforated by channels of the majority PS block with lower surface tension (40.7 dyn/cm) is also thermodynamically favored.[44] And hence, although the solvent used here has preferential affinity for the minority PMMA block, there is a very thin layer of PS (B1, 4−5 nm) covering the film surface, as shown in Figure 1a′. At the same time, in a solvent-cast film, a fast solvent evaporation rate will lead to bringing mechanical strain field with high strength.[12,45] The solvent evaporation rate $R \approx 0.01$ mL/h applied in the present work is fast enough to bring a strong mechanical strain field, which is expected to make the film shrinkage and accordingly the perforating channels close to fuse into ring-shaped morphologies. Therefore, the nature of the solvent together with the kinetics of the solvent evaporation is expected to be responsible for the interesting PLR microstructure as shown in Figures 1a and 1a′ formation. This conclusion is consistent with our previous work on the ring-shaped morphology formation in solution-cast block copolymer films by controlling solvent evaporation rate.[12]

Returning to the micrographs shown in Figure 1, when a solvent with lower preferential affinity for the minority PMMA block $\Delta\chi = -0.054$ was used, the degree of the swelling of the PMMA block resulted from the solvent is weaker than the solvent with $\Delta\chi = -0.063$, the effective volume fraction of the PS block will increase a little but not enough to change the essential microstructure, and hence a perforated lamellar microstructure with more PS channels perforating the PMMA layer as shown in the plane-view TEM micrograph in Figure 1b was observed. It looks like loose and tight rings and the width of the ring rods are also 50 ± 2 nm. The content of PS channels calculated from Figure 1b is ∼52%. And the thickness of B1, the dark PS layer at the film surface, calculated from the cross-sectional TEM micrograph of this film as shown in Figure 1b′ is ∼9 nm, which is thicker than that in the film prepared from the solvent with $\Delta\chi = -0.063$ as shown in Figure 1a′ (4−5

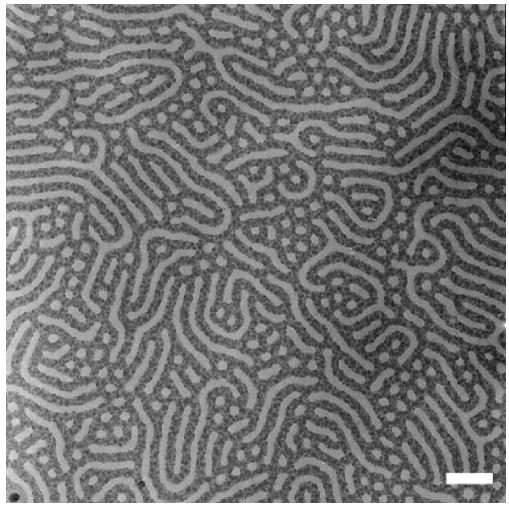

Figure 2. TEM micrograph of the film cast from the neutral solvent ($\Delta\chi = 0$) at the solvent evaporation rate $R \approx 0.01$ mL/h. Scale bar: 200 nm.

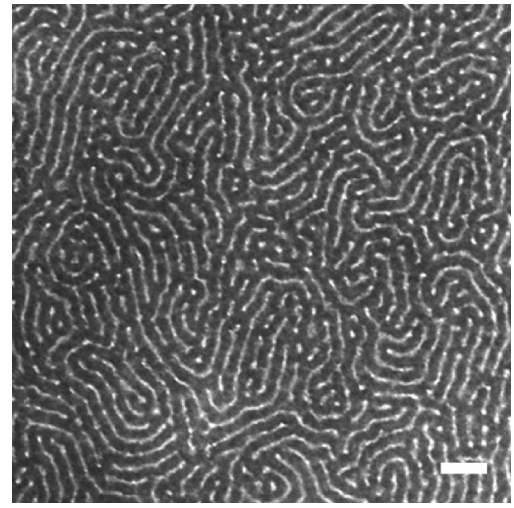

Figure 3. TEM micrograph of the film spin-coated from Tol annealed at 180 °C under vacuum for 48 h. Scale bar: 200 nm.

nm). Here, because the preferential affinity of the solvent for PMMA block decreases, it makes the PS block have more tendency to move to the film surface to increase the contact with the solvent.[46,47] On the other hand, the lower surface tension of PS block also makes it prefer to occupy the film surface to minimize the free energy. Therefore, the thickness of the PS covering the film surface increases.

As the preferential affinity of the solvent for the PMMA block decreases further to $\Delta\chi = -0.037$, the PS block occupies more space besides the space occupied by ring-rods. The perforated lamella with PS tail-attached ring-shaped morphology such as the microstructure shown in the plane-view TEM micrograph in Figure 1c was observed. The content of the PS channels increases to ~62%. The cross-sectional TEM micrograph as in Figure 1c′ shows that the PMMA layer is still perforated by the PS channels and the thickness of the dark PS layer at the film surface B1 is ~13 nm.

When the value $\Delta\chi = -0.020$, the microstructure changes from perforated lamella to cylinders as shown in the plane-view TEM micrograph in Figure 1d because the effective volume fraction of PMMA microdomain decreasing and not high enough to form perforated lamella. And in some places, parallel PMMA cylinders as shown in Figure 1d′ can be observed. As shown, the hybrid microstructure of PS rings and PS cylinders is expected to be the transitional microstructure from perforated lamella to cylinder phases.

$\Delta\chi = 0$: Neutral Solvent. Figure 2 shows the TEM micrograph of the block copolymer thin film cast from the neutral solvent ($\Delta\chi = 0$) at the solvent evaporation rate $R \approx 0.01$ mL/h. Obviously, the hybrid microstructure of PMMA cylinders and PMMA spheres formed. The period length of the dispersed PMMA microdomains is about ~77 nm, larger than that in the bulk, ~65 nm. A neutral solvent should diffuse into both two blocks equally and result in swelling both blocks to the same extent.[8] The microstructure of the films cast from the neutral solvent is expected to be similar to the spontaneous domain microstructure of the diblock copolymer with equal thickness subjected to thermal annealing treatment. To prove the expectation, thin film with thickness ~70 nm, similar to the solvent-cast film of the block copolymer, was prepared by spin-casting a 10 mg/mL solution in Tol onto carbon-coated mica at 2000 rpm for 30 s. After removal of the residual solvent the film was annealed at 180 °C under vacuum for 48 h. The plane-view TEM micrograph of the spontaneous domain microstructure of the film was shown in Figure 3. It shows clearly that the hybrid microstructure consists of short PMMA cylinders and PMMA spheres, similar to the microstructure formed in the film cast from the neutral solvent $\Delta\chi = 0$ as shown in Figure 2. The period length of the dispersed PMMA microdomains is about ~67 nm, similar to that in the bulk ~65 nm.

Although the microstructures of the films prepared by solvent-casting in Figure 2 and thermal-annealing in Figure 3 are similar, the period length of the former ~77 nm is larger than that of the latter ~67 nm. A neutral solvent is expected to swell both blocks and increases the period of the microdomain spacing in solution, and such a state can be held in the film by the fast evaporation of the solvent. When the film is subjected to thermal annealing, however, each block keeps its size as those in bulk. Therefore, the period length of the microdomains in neutral solvent casting film is larger than that in the bulk, but that in thermal annealing film is similar to that in the bulk. That is, a neutral solvent changes the period length of the block copolymer, but the shape of the microstructure keeps invariable. This is consistent with the reference 33.

$\Delta\chi > 0$: The Solvents Have Preferential Affinity for the Majority PS Block. Figure 4 shows the TEM micrographs of the block copolymer thin films cast from the solvents with preferential affinity for the majority PS block ($\Delta\chi > 0$) at evaporation rate $R \approx 0.01$ mL/h. Since the solvent has preferential affinity for the majority PS block, it makes the degree of the swelling of the PS block higher than that of the PMMA block, and accordingly the effective volume fraction of PS block is higher than that in the bulk. Therefore, a microstructure of PMMA spheres dispersing in a PS matrix as shown in the plane-view TEM micrograph in Figure 4a and the cross-sectional TEM micrograph in Figure 4a′ were obtained as the solvent with $\Delta\chi = 0.021$ is used. With the solvent preferential affinity for PS block increasing further to $\Delta\chi = 0.030$ (pure Tol), the PMMA block forms parallel cylinders again, as shown in the plane and cross-sectional TEM micrographs in Figure 4 panels b and b′, respectively. It is an unconventional phase transition from PMMA spherical phase as shown in Figure 4a,a′ to PMMA cylindrical phase as shown in Figure 4b,b′ as the solvent preferential affinity for the majority PS block increases from $\Delta\chi = 0.021$ to $\Delta\chi = 0.030$. But the cross-sectional TEM micrograph in Figure 4b′ shows that there is a thick layer of dark PS, ~25 nm, much thicker than that in

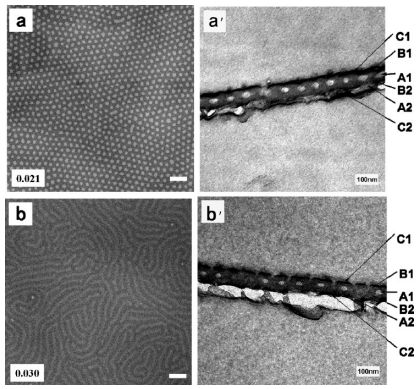

Figure 4. TEM micrographs of the films cast from the solvents with preferential affinity for PS block ($\Delta\chi > 0$) at the solvent evaporation rate $R \approx 0.01$ mL/h. The preferential affinities of the solvents are (a and a′) 0.021 and (b and b′) 0.030. The panels a′ and b′ show the cross-sectional TEM micrographs corresponding to plane-view micrographs in panels a and b, respectively. Scale bar for the plane-view micrographs: 200 nm.

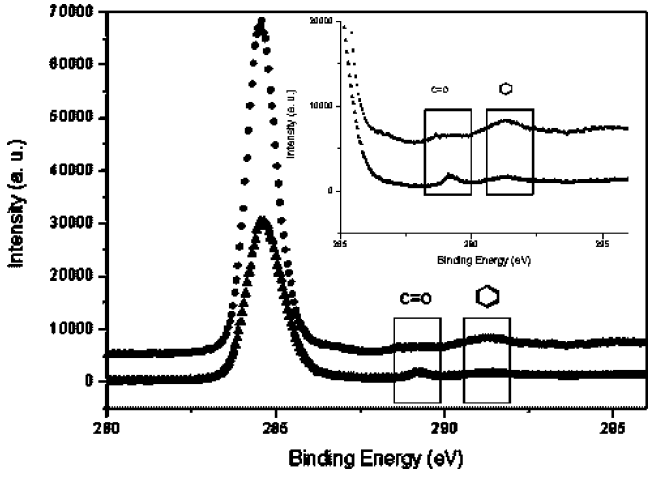

Figure 5. XPS C1s spectra of the film cast from the solvents with different preferential affinity at the solvent evaporation rate $R \approx 0.01$ mL/h. The preferential affinities of the solvents are (▲) −0.037 and (●) 0.030, respectively. For clarity, the trace black dot for $\Delta\chi = 0.030$ is offset by 5000 in intensity.

Figure 4a′, ∼16 nm, covering the film surface. The nature of the solvent is still expected to play a key role. Since the solvent with $\Delta\chi = 0.030$ has more preferential affinity for the majority PS block, the effective volume fraction of PS increases more, and simultaneously more PS moves to the surface of the film to increase the contact with the solvent.[46,47] Hence, the PS microdomain remaining in the film bulk decreases, and accordingly the PMMA microdomain forms a parallel cylindrical phase dispersing in a PS matrix.

The confirmation of the thickness increase of the PS layer at the film surface with increasing the casting solvent preferential affinity for PS is obtained by XPS. Figure 5 shows the profiles of relative photoelectron intensity of C1s as a function of binding energy for the films cast from the binary solvent mixtures with $\Delta\chi = -0.037$ and 0.030, respectively. The profiles have been normalized on the peak of C−C bond with a binding energy of 284.5 eV. For clarity, trace for $\Delta\chi = 0.030$ is offset by 5000 in intensity. We can clearly see the relatively high carbonyl group peak at 288.8 eV for the film obtained from the solvent with $\Delta\chi = -0.037$ in Figure 5, implying the thickness of the PS layer at the film surface is very thin. With increasing the value of $\Delta\chi$ from −0.037 to 0.030, the carbonyl group peak at 288.8 eV decreases but the phenyl ring peak at 291.3 eV increases, indicating the thickness of the PS layer at the film surface increases. This is consistent with the results obtained by TEM: the thickness of the dark PS layer at the top of the film is ∼13 nm for the film obtained from $\Delta\chi = -0.037$ as shown in Figure 1c′ and that is ∼25 nm for the film obtained from $\Delta\chi = 0.030$ as shown in Figure 4b′.

On the other hand, comparing with large amount of PS moving to the film surface induced by the casting solvent preferential affinity at $\Delta\chi > 0$, the amount of PMMA moving to the film surface induced by the solvent preferential affinity at $\Delta\chi < 0$ is less, even when the value of $|\Delta\chi|$ is high enough. The occurrence of this phenomenon is attributed to the quantity of each block and the carbon-coated mica substrate. The carbon-coated mica substrate preference for the higher surface tension PMMA block makes some of the minority PMMA block move to the carbon-coated mica substrate. Therefore, there is not enough PMMA block moving to the surface at $\Delta\chi < 0$. On the contrary, the PS block can move to the surface when $\Delta\chi > 0$; even the surface of all the film obtained from any preferential affinity solvent is covered by a layer of PS in the present work. Especially, the layer of PS changes the microstructure of the film prepared from the solvent with $\Delta\chi = 0.030$, as shown in Figure 4b′.

Conclusions

The microstructures of cylinder-forming PS-*b*-PMMA diblock copolymer thin films with a thickness of about 70−80 nm cast from TCE, Tol, and their binary solvent mixtures at a certain solvent evaporation rate $R \approx 0.01$ mL/h have been investigated. With increasing the preferential affinity of the solvents for the majority PS block gradually, the microstructures including perforated lamella with ring-like morphologies, PMMA cylinders, PMMA spheres, and PMMA cylinders covered with a layer of PS microdomain were obtained. When the solvent preferential affinity $\Delta\chi$ is between −0.063 and −0.020, the microstructures of perforated lamella with ringlike morphologies were obtained. The formation of the special microstructures of perforated lamella was explained by the preferential affinity of solvents and the special mechanical strain field brought by the solvent evaporation rate $R \approx 0.01$ mL/h. When $\Delta\chi = 0$, a neutral solvent for the diblock copolymer, the hybrid microstructure of PMMA cylinders and spheres dispersing in a PS matrix were observed. It is consistent with the spontaneous equilibrium microstructure of the diblock copolymer since the neutral solvent diffuses into both blocks equally and results in swelling both blocks to equal extent. When $\Delta\chi > 0$, the microstructures of PMMA spheres and PMMA cylinders covered with a layer of PS microdomain formed because the solvent shows preferential affinity for the majority PS block and the quantity of the PS block favors movement to the surface. The results indicate that the solvent preferential affinity which influences the effective volume fraction of each block and the special mechanical strain field brought by the solvent evaporation rate play a crucial role in the complex microstructures formation.

Acknowledgment. We are grateful to Ms. Guifen Sun for technical help with the microtomy. This work is supported by National Natural Science Foundation of China (Grant 20774095).

References and Notes

(1) Hamley, I. W. *The Physics of Block Copolymers*; Oxford University Press: New York, 1998.
(2) Abetz, V.; Simon, P. F. W. *Adv. Polym. Sci.* **2005**, *189*, 125.

(3) Fasolka, M. J.; Mayes, A. M. *Annu. Rev. Mater. Res.* **2001**, *31*, 323.
(4) Hamley, I. W. *Nanotechnology* **2003**, *14*, R39–R54.
(5) Förster, S.; Plantenberg, T. *Angew. Chem., Int. Ed.* **2002**, *41*, 688.
(6) Olson, D. A.; Chen, L.; Hillmyer, M. A. *Chem. Mater.* **2008**, *20*, 869.
(7) Inoue, T.; Soen, H.; Hashimoto, T.; Kawai, H. *J. Polym. Sci., A2* **1969**, *7*, 1283.
(8) Funaki, Y.; Kumano, K.; Nakao, T.; Jinnai, H.; Yoshida, H.; Kimishima, K.; Tsutsumi, K.; Hirokawa, Y.; Hashimoto, T. *Polymer* **1999**, *40*, 7147.
(9) Kim, G.; Libera, M. *Macromolecules* **1998**, *31*, 2569.
(10) Knoll, A.; Horvat, A.; Lyakhova, K. S.; Krausch, G.; Sevink, G. J. A.; Zvelindovsky, A. V.; Magerle, R. *Phys. Rev. Lett.* **2002**, *89*, 035501.
(11) Fukunaga, K.; Elbs, H.; Magerle, R.; Krausch, G. *Macromolecules* **2000**, *33*, 947.
(12) Gong, Y.; Hu, Z.; Chen, Y.; Huang, H.; He, T. *Langmuir* **2005**, *21*, 11870.
(13) Gong, Y.; Huang, H.; Hu, Z.; Chen, Y.; Chen, D.; Wang, Z.; He, T. *Macromolecules* **2006**, *39*, 3369.
(14) Huang, H.; Zhang, F.; Hu, Z.; Du, B.; He, T.; Lee, F. K.; Wang, Y.; Tsui, O. K. C. *Macromolecules* **2003**, *36*, 4084.
(15) Huang, H.; Hu, Z.; Chen, Y.; Zhang, F.; Gong, Y.; He, T.; Wu, C. *Macromolecules* **2004**, *37*, 6523.
(16) Zhang, Q.; Tsui, O. K. C.; Du, B.; Zhang, F.; Tang, T.; He, T. *Macromolecules* **2000**, *33*, 9561.
(17) Chen, Y.; Huang, H.; Hu, Z.; He, T. *Langmuir* **2004**, *20*, 3805.
(18) Chen, Y.; Wang, Z.; Gong, Y.; Huang, H.; He, T. *J. Phys. Chem. B* **2006**, *110*, 1647.
(19) Guo, R.; Huang, H.; Chen, Y.; Gong, Y.; Du, B.; He, T. *Macromolecules* **2008**, *41*, 890.
(20) Guo, R.; Huang, H.; Du, B.; He, T. *J. Phys. Chem. B* **2009**, *113*, 2712.
(21) Morkved, T. L.; Lu, M.; Urbas, A. M.; Ehrichs, E. E.; Jaeger, H. M.; Russell, T. P. *Science* **1996**, *273*, 931.
(22) Thurn-Albrecht, T.; Schotter, J.; Kästle, G. A.; Emley, N.; Shibauchi, T.; Krusin-Elbaum, L.; Guarini, K.; Black, C. T.; Tuominen, M. T.; Russell, T. P. *Science* **2000**, *290*, 2126.
(23) Knoll, A.; Magerle, R.; Krausch, G. *J. Chem. Phys.* **2004**, *120*, 1105.
(24) Tsarkova, L.; Knoll, A.; Krausch, G.; Magerle, R. *Macromolecules* **2006**, *39*, 3608.
(25) Zoelen, W. V.; Asumaa, T.; Ruokolainen, J.; Ikkala, O.; Brinke, G. T. *Macromolecules* **2008**, *41*, 3199.
(26) Zoelen, W. V.; Polushkin, E.; Brinke, G. T. *Macromolecules* **2008**, *41*, 8807.
(27) Sperschneider, A.; Schacher, F.; Gawenda, M.; Tsarkova, L.; Müller, A. H. E.; Ulbricht, M.; Krausch, G.; Köhler, J. *Small* **2007**, *3*, 1056.
(28) Ludwigs, S.; Schmidt, K.; Krausch, G. *Macromolecules* **2005**, *38*, 2376.
(29) Ludwigs, S.; Böker, A.; Voronow, A.; Rehse, N.; Magerle, R.; Krausch, G. *Nat. Mater.* **2003**, *2*, 744.
(30) Park, I.; Park, S.; Park, H. W.; Chang, T.; Yang, H.; Ryu, C. Y. *Macromolecules* **2006**, *39*, 315.
(31) Bang, J.; Kim, B. J.; Stein, G. E.; Russell, T. P.; Li, X.; Wang, J.; Kramer, E. J.; Hawker, C. J. *Macromolecules* **2007**, *40*, 7019.
(32) Sriprom, W.; James, M.; Perrier, S.; Neto, C. *Macromolecules* **2009**, *42*, 3138.
(33) Jung, Y. S.; Ross, C. A. *Adv. Mater.* **2009**, *21*, 2540.
(34) Yang, Y.; Qiu, F.; Zhang, H.; Yang, Y. *Polymer* **2006**, *47*, 2205.
(35) Chen, P.; Liang, H.; Shi, A.-C. *Macromolecules* **2007**, *40*, 7329.
(36) Almdal, K.; Koppi, K. A.; Bates, F. S.; Mortensen, K. *Macromolecules* **1992**, *25*, 1743.
(37) Hamley, I. W.; Koppi, K. A.; Rosedale, J. H.; Bates, F. S.; Almdal, K.; Mortensen, K. *Macromolecules* **1993**, *26*, 5959.
(38) Förster, S.; Khandpur, A. K.; Zhao, J.; Bates, F. S.; Hamley, I. W.; Ryan, A. J.; Bras, W. *Macromolecules* **1994**, *27*, 6922.
(39) Khandpur, A. K.; Förster, S.; Bates, F. S.; Hamley, I. W.; Ryan, A. J.; Almdal, K.; Mortensen, K. *Macromolecules* **1995**, *28*, 8796.
(40) Schulz, M. F.; Khandpur, A. K.; Bates, F. S.; Almdal, K.; Mortensen, K.; Hajduk, D. A.; Gruner, S. M. *Macromolecules* **1996**, *29*, 2857.
(41) Hajduk, D. A.; Takenouchi, H.; Hillmyer, M. A.; Bates, F. S.; Vigild, M. E.; Almdal, K. *Macromolecules* **1997**, *30*, 3788.
(42) Van Krevelen, D. W. *Properties of Polymers*; Elsevier Scientific Publishing. Company: New York, 1976.
(43) Brandrup, J.; Immergut, E. H.; Grulke, E. A. *Polymer Handbook*, 4th ed.; John Wiley & Sons: New York, 1999.
(44) Green, P. F.; Christensen, T. M.; Russell, T. P.; Jérôme, R. *Macromolecules* **1989**, *22*, 2189.
(45) Rabani, E.; Reichman, D. R.; Geissler, P. L.; Rrus, L. E. *Nature* **2003**, *426*, 271.
(46) Gong, Y.; Joo, W.; Kim, Y.; Kim, J. K. *Chem. Mater.* **2008**, *20*, 1203.
(47) Xu, T.; Stevens, J.; Villa, J. A.; Goldbach, J. T.; Guarini, K. W.; Black, C. T.; Hawker, C. J.; Russell, T. P. *Adv. Funct. Mater* **2003**, *13*, 698.
(48) Cheng, N. *Solvents Handbook*; Chemical Industry Press: Beijing, China, 2008.

JP908852U